Proof-of-principle demonstration of vertical-gravity-gradient measurement using a single-proof-mass double-loop atom interferometer

I. Perrin, Y. Bidel, N. Zahzam, C. Blanchard, and A. Bresson
DPHY, ONERA, Université Paris Saclay, F-91123 Palaiseau, France

M. Cadoret*
LCM-CNAM, 61 rue du Landy, 93210, La Plaine Saint-Denis, France

(Received 14 October 2018; published 2 January 2019)

We demonstrate a proof-of-principle of direct Earth gravity-gradient measurement with an atom interferometer-based gravity gradiometer using a single proof mass of cold ^{87}Rb atoms. The atomic gradiometer is implemented in the so-called double-loop configuration, hence providing a direct gravity-gradient dependent phase shift insensitive to dc acceleration and constant rotation rate. The atom interferometer (AI) can be either operated as a gravimeter or a gradiometer by simply adding an extra Raman π pulse. We demonstrate gravity-gradient measurements first using a vibration isolation platform and second without seismic isolation using the correlation between the AI signal and the vibration signal measured by an auxilliary classical accelerometer allowing one to bypass the absence of common-mode vibration noise rejection in a double-loop geometry. The simplicity of the experimental setup (a single atomic source and unique detection) and the immunity of the AI to rotation-induced contrast loss make it a possible candidate for onboard gravity-gradient measurements.

DOI: 10.1103/PhysRevA.99.013601

I. INTRODUCTION

Light-pulse atom interferometers (AIs) use short pulses of light to split, redirect, and then recombine cold atoms used as a matter-wave source. Since their advent in the 1990s [1,2], they have demonstrated to be extremely sensitive and accurate sensors very useful in fundamental physics research where they have been used to measure fundamental constants [3–6], test the equivalence principle [7–11], put bounds on theories of dark energy [12], and probe quantum superposition at the macroscopic level [13], as well as measuring gravitoinertial force such as gravity acceleration [14–18], rotations [19–22], and gravity gradient [23–26]. Most of these works consist in laboratory experiments but atom interferometer's inherent long-term stability and accuracy have led to a global push towards performing experiments outside the laboratory environment [17,27,28]. Moreover, cold atom–based gravity sensors have started to be commercialized, hence targeting out of the laboratory applications. In this context, development of gravity gradiometers are also particularly attractive as they complement pure gravity measurements and find variety of applications including geodesy [29], geophysics [30], and inertial navigation [31] for which the required performances are around $10\,\mathrm{E}/\sqrt{\mathrm{Hz}}$ for terrestrial instruments and around a few $\mathrm{mE}/\sqrt{\mathrm{Hz}}$ for space instruments. Whereas an atomic gravimeter sensitivity is often limited by vertical vibration noise, this is not the case in a conventional atomic gradiometer where the gravity gradient is derived from the differential measurement of two simultaneous atom interferometers performed at two locations. However, this requires one to use two clouds of cold atoms spatially separated. This can for example be achieved by using laser-cooled atomic sources originating from two separate three-dimensional magneto-optical traps (3D-MOT) [23], or by launching the atoms from a single MOT using moving molasses [24] or Bloch oscillations as an atomic elevator [32,33] or using large momentum transfer (LMT) beam splitters combining Bragg pulse and Bloch oscillations [34]. Although these techniques have proven to work in a laboratory environment, their complexity could still be an issue regarding their implementation for onboard applications where simple and compact instruments are required. In this paper, we perform a *proof-of-principle* experimental demonstration of an alternative method consisting in a direct measurement of the vertical gravity gradient with only one source of cold 87 rubidium atoms in the presence of vibration noise. We use a double-loop four-pulse AI geometry as proposed initially in [35] for gravity-gradient measurements which was investigated in [23,36] and now used in several experiments such as rotation rate measurements in atomic fountain configurations [22,37] or for low-frequency vibration noise rejection in the context of airborne tests of the weak equivalence principle (WEP) using atom interferometry [27]. We perform vertical-gravity-gradient measurement with and without a passive isolation vibration platform and show that in the presence of parasitic ground vibrations the correlation of the vibration signal measured by a classical accelerometer [32,38,39] allows one to recover the interference fringes and extract the vertical gravity gradient. Moreover, we make a study of the systematics when using this double-loop AI geometry. The paper is organized as follows. Section II presents the double loop four-pulse AI used to measure the vertical gravity gradient. Section III presents the experimental setup. Section IV describes the vertical-gravity-gradient

*malo.cadoret@lecnam.net

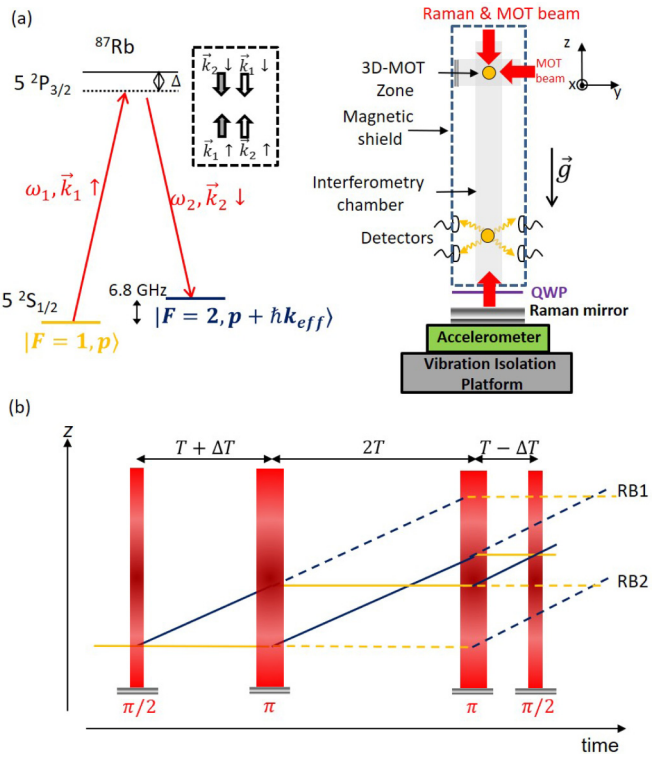

FIG. 1. (a) Left: energy level scheme of rubidium $D2$ line. Two-photon Raman transitions performed on a single cloud of 87 rubidium atoms in vertical configuration. (Δ is the one photon detuning from the electronic transition.) Right: schematic of the experimental setup. The Raman laser beams are aligned along gravitational acceleration g. PD: photodiode. (b) Space-time recoil diagram in the absence of gravity of the four pulse double-loop AI based gravity gradiometer. A time asymmetry ΔT is implemented to suppress parasitic Ramsey-Bordé interferometers (labeled RB1 and RB2 on figure) (dash line) due to imperfect mirror pulses.

measurement performing the AI with a passive vibration isolation platform and Sec. V presents the measurement without seismic isolation, using the correlation technique. Section VI presents a study of the major systematic effects which affect the measurement. Finally, in Sec. VII, a discussion on scale factor comparisons between dual cloud AI versus single cloud four LPAI is made and possible improvements of the measurement are presented.

II. FOUR PULSE ATOM INTERFEROMETER-BASED GRAVITY GRADIOMETER

We consider a four pulse AI. The matter-wave beam splitters and mirrors are based on two-photon counterpropagative Raman transitions between the $F = 1$ and $F = 2$ hyperfine ground states of rubidium 87 atoms [see Fig. 1(a)]. An atom initially in state $|F = 1, p\rangle$ is coupled to state $|F = 2, p + \hbar k_{\text{eff}}\rangle$, where $\hbar k_{\text{eff}}$ is the two-photon momentum transfer. Here $\vec{k}_{\text{eff}} = \vec{k}_1 - \vec{k}_2$ is the effective wave vector (with $\|\vec{k}_{\text{eff}}\| = \|\vec{k}_1\| + \|\vec{k}_2\|$ for counterpropagative transitions). The AI consists of the light-pulse sequence $(\pi/2 - \pi - \pi - \pi/2)$ which differs from a usual Mach-Zehnder atomic gravimeter by the presence of an additional π pulse and a different time sequence. Practically, a first $\pi/2$ pulse creates an equal superposition of ground ($F = 1$) and excited ($F = 2$) states. Then, two π pulses redirect the two atomic paths letting the wave packets cross each other in between, and a final $\pi/2$ pulse interferes the wave packets. Thus this sequence leads to a double-loop geometry. In our configuration, $\vec{k}_{\text{eff}}$ is aligned with the local gravity acceleration $\vec{g}$, for all Raman pulses. This sequence allows one to measure the time derivative of the acceleration of the free-falling atoms.

Although a symmetric configuration is necessary to fully cancel the phase contribution due to constant acceleration [40], a time asymmetry ΔT is introduced to avoid interference of parasitic Ramsey-Bordé interferometers due to imperfect π pulses [22]; see Fig. 1(b). In the absence of time asymmetry, these parasitic interferometers would close at the same time as the main interferometer and generate amplitude noise and a possible bias on the gravity-gradient determination. In the short, intense-pulse limit, the phase shift along the Raman laser direction of propagation is expressed as [40]

$$\begin{aligned}\Delta\Phi &= 4(k_{\text{eff}} g - \alpha) T \Delta T - (2k_{\text{eff}} v_z T^3 + 4k_{\text{eff}} g T^4)\Gamma_{zz} \\ &\quad + 4k_{\text{eff}} a_{\text{vib}} T \Delta T - 2k_{\text{eff}} \dot{a}_{\text{vib}} T^3 \\ &\equiv \varphi_g + \varphi_{\text{grad}} + \varphi_{\text{vib}}, \end{aligned} \tag{1}$$

where g is the Earth gravity acceleration along the Raman laser beams, α the radio-frequency chirp rate applied to the effective Raman frequency to compensate the Doppler shift induced by the atom free fall in order to keep resonance, Γ_{zz} the vertical-gravity-gradient component, v_z the initial atomic velocity along the vertical z axis at the first Raman pulse, a_{vib} the mirror acceleration, $\dot{a}_{\text{vib}}$ its time derivative, and T the time between the Raman $\pi/2$ and π pulses in the absence of timing asymmetry. In Eq. (1), the contribution to the phase shift contains three separate terms. The first term φ_g is a remaining sensitivity to gravity acceleration induced by the timing asymmetry ΔT. We have embedded the laser phase $\alpha T \Delta T$ in this term. The second term is the gravity-gradient-dependent phase shift φ_{grad} and finally the third term is the phase shift induced by vibrations which we denote φ_{vib}. This vibrational phase noise may prevent one from discriminating spatial acceleration variations from time varying acceleration variations, and remains an issue for gravity-gradient measurements performed in this double-loop geometry. Nevertheless, to circumvent this problem the AI can be operated using a passive vibration isolation platform ($\varphi_{\text{vib}} \simeq 0$) or by estimating the φ_{vib} phase term induced by the Raman mirror vibration using the acceleration noise recorded by an auxiliary classical accelerometer rigidly fixed to the Raman mirror. We have operated the AI using these two schemes. For both schemes the atomic gradiometer is operated in its most sensitive configuration with $T = 38,6$ ms limited by the falling distance (see Sec. III), a timing asymmetry $\Delta T = 300\ \mu$s, and an initial velocity at first Raman pulse $v_z = 0.38$ m/s, leading to phase-shift values reported in Table I. The time asymmetry has been chosen experimentally to avoid the extra RB interferometers to form fringes, thus maximizing the signal-to-noise ratio of the AI. For our application we have neglected the effect of the recoil phase shift.

TABLE I. Phase-shift terms of numerical values assuming the following: $k_{\text{eff}} = \frac{4\pi}{\lambda} = 1.61\times10^{7}\,\text{m}^{-1}$ with $\lambda = 780$ nm the wavelength of the transition, vertical Earth gravity gradient $\Gamma_{zz} = 3.1\times10^{-6}\,\text{s}^{-2}$ (assuming a spherical symmetric Earth) with $g = 9.81\,\text{m}\,\text{s}^{-2}$, interferometer pulse timing asymmetry of $\Delta T = 300\ \mu$s, $T = 38.6$ ms, and initial velocity $v_z = 0.38\,\text{ms}^{-1}$. The last term correponds to the recoil phase shift ($v_r = 5.89\,\text{mm}\,\text{s}^{-1}$). The gravimeter phase-shift term is taken as reference.

Phase term	Absolute numeric value (mrad)	Relative phase
$4k_{\text{eff}}gT\Delta T$	7.3×10^{6}	1
$4k_{\text{eff}}\Gamma_{zz}gT^{4}$	4.3	6×10^{-7}
$2k_{\text{eff}}\Gamma_{zz}v_zT^{3}$	2.2	3×10^{-7}
$k_{\text{eff}}\Gamma_{zz}v_rT^{3}$	1.7×10^{-2}	2×10^{-9}

III. EXPERIMENTAL SETUP

In this section we describe the main parts of the apparatus as well as the time sequence of the experiment.

A. Apparatus overview

Our experimental setup is schematically shown in Fig. 1. It consists of a titanium vacuum chamber where the atoms are produced and interrogated and to which are connected ion pumps, getters, and rubidium dispensers. The vacuum chamber is magnetically shielded with two cylindrical layers of μ metal. The cold atom source is produced at the top of the chamber using a 3D MOT configuration. The falling distance available for interferometry is 20 cm from the MOT. The two counterpropagating Raman beams are obtained with a phase-modulated laser at 6.8 GHz retroreflected on a mirror (Raman mirror). The Raman laser beams enter the vacuum chamber through the top window. After passing through a quarter wave plate they are retroreflected by the Raman mirror at the bottom of the setup, outside the vacuum, in order to realize the counterpropagating configuration, thus obtaining a lin $\perp$ lin configuration in the AI region. In this configuration, two pairs of counterpropagating Raman beams ($\uparrow \vec{k}_1, \downarrow \vec{k}_2$ and $\downarrow \vec{k}_1, \uparrow \vec{k}_2$) in the vertical direction are present. Degeneracy between the two pairs of Raman beams is lifted through Doppler shift induced by gravity during free fall of the atoms. In this configuration, only the Raman mirror needs to be isolated from ground vibrations. In our setup the mirror is rigidly linked to a classical accelerometer (Titan Nanometrics), the whole being fixed to a passive vibration isolation platform (Minus-K).

B. Optical setup

The laser system used for cooling, detecting, and driving the interferometer pulses is similar to the one described in [41]. Basically, it consists in a compact and robust laser system based on a single narrow linewidth Erbium doped fiber laser at 1.5 μm, amplified in a 5 W Erbium doped fiber amplifier (EDFA) and then frequency doubled in a periodically poled lithium niobate (PPLN) crystal. A power of 450 mW is available at 780 nm. The Raman laser and the repumper are generated thanks to a fiber phase modulator at 1.5 μm, allowing one to be free from any phase lock loop between the two Raman lines.

C. Experimental sequence

The experimental sequence of the atomic gradiometer is the following: first, a cold ^{87}Rb sample is produced in a three-dimensional MOT, loaded from a background vapor pressure of $\sim10^{-8}$ mbar. After 700 ms of trap loading, a stage of optical molasses, and a microwave selection, we assemble $N_{at} \sim 5\times10^{7}$ atoms in the magnetic insensitive ground state $|F = 1, m_F = 0\rangle$ at a temperature $\Theta = 3\ \mu$K. A push beam gets rid of the atoms left in state $F = 2$. Then, after 38.6 ms of free fall, we apply the AI sequence consisting in four Raman laser pulses of 8, 16, 16, and 8 μs. This time delay before the first Raman pulse is necessary to first lift degeneracy between the two pairs of Raman beams and second to minimize the impact of parasitic Raman lines (see Sec. VI). During the AI operation a bias magnetic field of 100 mG is applied. We set $T = 38.6$ ms corresponding to total interrogation time $4T = 154.4$ ms. Following the interferometer sequence we measure the proportion of atoms in the two output ports $F = 2$ and $F = 1$ of the interferometer using state selective vertical light-induced fluorescence detection. The fluorescence is collected thanks to collimation lenses and photodiodes in the perpendicular direction. The measurement of the proportion of atoms P in the state $F = 2$ at the exit of the interferometer is a sinusoidal function of the interferometric phase shift:

$$P = P_m + \frac{C}{2}\cos(\Delta\Phi), \tag{2}$$

where P_m is the fringe offset and C the fringe contrast which is in our case $C = 0.1$. Interferometric fringes are thus obtained through scanning the interferometric phase. In our experiment we operate the interferometer with and without a vibration isolation platform. Therefore, a scanning of the phase is obtained first by varying the frequency chirp rate of the Raman laser and second by letting vibration noise operate a random sampling of the interferometric phase. The repetition rate of the experimental sequence is 1 Hz, including atom loading, state preparation, atom interferometry, and state detection. The whole experimental sequence timing and data acquisition is computer controlled.

IV. GRAVITY-GRADIENT MEASUREMENT WITH VIBRATION ISOLATION

In this section we present the vertical-gravity-gradient measurement when operating the AI with a vibration isolation platform.

A. Measurement method

To measure the vertical gravity gradient we take advantage of the acceleration sensitivity induced by the timing asymmetry ΔT of the interferometer. In the presence of a vibration isolation platform ($\varphi_{\text{vib}} \approx 0$), interferometer fringes can be obtained by scanning the frequency chirp α. The interference phase is obtained using the fringe-locking method (FLM) similar to the one described in [17], which determines the frequency chirp nulling the phase. The sign of the

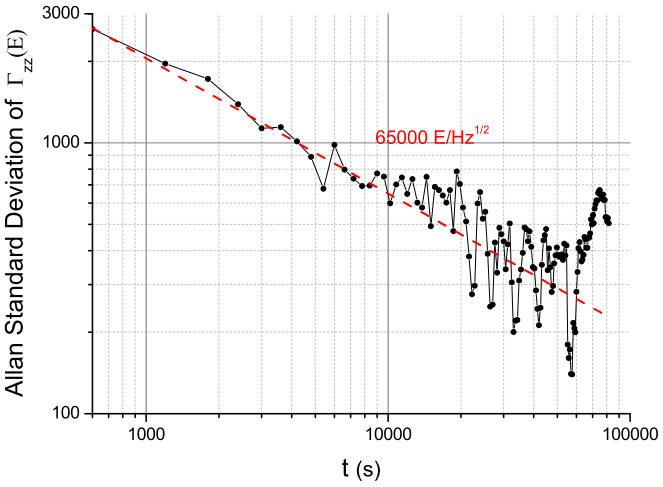

FIG. 2. Allan standard deviation of the gravity-gradient measurements. The dash line illustrates the $t^{-1/2}$ scaling.

radio-frequency chirp is changed every two drops, hence reversing the sign of $\vec{k}_{\text{eff}}$ to cancel some systematic effects. Nevertheless, in our protocol, we suppress sensitivity to gravity acceleration by periodically reversing the sign of ΔT (every 5 min), hence reversing the sign of the acceleration phase shift in Eq. (1). Nulling the phase shift in both configurations and taking the mean value leads to

$$\Gamma_{zz} = \frac{2T\Delta T(\alpha_-^0 - \alpha_+^0)}{2k_{\text{eff}}v_z T^3 + 4k_{\text{eff}}gT^4}, \tag{3}$$

where α_+^0 (α_-^0) is the frequency chirp which nulls the phase for ΔT ($-\Delta T$), respectively.

B. Gradiometer sensitivity

We have operated the gravity gradiometer continuously during 2 days using the experimental sequence decribed in Sec. III C. The time asymmetry ΔT is changed every 5 minutes. We obtained from Eq. (3) the uncorrected vertical-gravity-gradient mean value $\Gamma_{zz} = 7600$ E. The Allan standard deviation (ADEV) on the gravity-gradient measurements is shown on Fig. 2. Each point corresponds to the measurements averaged over 10 min. corresponding to the time necessary to operate the AI in two configurations ($+\Delta T$ and $-\Delta T$). A short-term sensitivity of 65000 E/$\sqrt{\text{Hz}}$ is obtained during the two days of measurements. The stability of the gravity-gradient measurement improves as $t^{-1/2}$ (where t is the measurement time) and reaches 766 E after 2 h. The sensitivity of the single proof-mass atomic gradiometer still remains beyond state of the art atomic gradiometer using two simultaneous accelerometers with two proof masses in differential mode [23,24,26]. The sensitivity of our measurement is not limited by the contribution of residual vibration noise which has been measured with our low noise accelerometer at the level of 10000 E/$\sqrt{\text{Hz}}$, nor by detection noise which has been estimated at the level of 9500 E/$\sqrt{\text{Hz}}$, with a calculated quantum projection noise (QPN) of 4200 E/$\sqrt{\text{Hz}}$ for $\sim 5\times 10^6$ atoms. The other technical noise sources (microwave phase noise, laser frequency noise, Raman pulses intensity fluctuations, etc.) which may limit the sensitivity of the measurement have not been studied. We have investigated the main systematic effects which induce a bias on the gravity-gradient measured value using this method. These systematics are presented in Sec. VI.

V. GRAVITY-GRADIENT MEASUREMENT USING THE CORRELATION TECHNIQUE

In this section we present gravity-gradient measurement in the presence of vertical vibration noise.

A. Measurement method

First the vibration isolation platform on which is fixed the Raman mirror is made nonfloating. In the absence of vibration isolation $\varphi_{\text{vib}} \neq 0$ in Eq. (1); thus the conventional FLM used in Sec. IV A is not applicable anymore as it requires phase fluctuations to be smaller than π. To circumvent the presence of vibration excess noise which washes out fringe visibility, we perform a correlation-based technique [38,42] combining the simultaneous measurements of the output signal P of our interferometer and the one from a classical accelerometer fixed to the Raman mirror (see Fig. 1). The method is the following. First we held the laser phase fixed by setting the radio-frequency chirp α_0 to its value compensating for gravity acceleration leading to $\varphi_g = 0$. This value of α_0 is determined by operating the interferometer as a conventional three-pulse Mach-Zehnder interferometer using $T = 81.9$ ms (where T is the time between two-consecutive Raman pulses). Second, the AI is operated with the same experimental sequence except that the radio-frequency chirp sign is changed every measurement cycle. The atomic fringes are scanned due to random vibration noise. The probability P of the interferometer is plotted versus the estimated induced vibration phase φ_{vib}^E, which is numerically calculated at each cycle by convoluting the mirror acceleration $a_M(t)$ measured by the classical accelerometer, with the time response function $h_{at}(t)$ of the AI:

$$\varphi_{\text{vib}}^E = k_{\text{eff}} \int a_M(t) h_{at}(t) dt, \tag{4}$$

where h_{at} is a double triangle–like function represented on Fig. 3 defined as

$$h_{at}(t) = \begin{cases} \frac{t}{T^2} & \text{if} \quad 0 < t < T + \Delta T, \\ \frac{2(T+\Delta T)-t}{T^2} & \text{if} \quad T + \Delta T < t < 3T + \Delta T, \\ \frac{t-4T}{T^2} & \text{if} \quad 3T + \Delta T < t < 4T, \\ 0 & \text{otherwise.} \end{cases} \tag{5}$$

Finally, we perform a sinusoidal least-square fit of the data using the function

$$P = A + \frac{B}{2}\cos\left(\varphi_{\text{vib}}^E + \delta\phi\right), \tag{6}$$

where A, B, and $\delta\phi$ are free parameters. Performing a measurement of the transition probability in four configurations ($\vec{k}_{\text{eff}} \uparrow, \downarrow, \pm\Delta T$), where reversing the sign of $\vec{k}_{\text{eff}}$ (e.g., changing the sign of α) allows one to reject some systematics, and reversing the sign of ΔT suppresses residual dependence to constant acceleration, one can obtain the gravity gradient.

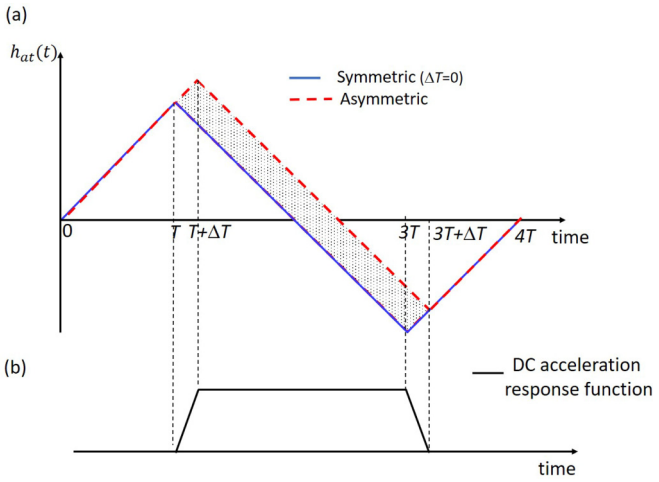

FIG. 3. (a) Four pulse AI response function h_{at} neglecting pulse duration for a symmetric (solid line) and asymmetric (dash line) configuration. (b) Response function of the residual sensitivity to dc acceleration is obtained from the difference between asymmetric and symmetric four pulse AI response functions.

B. Experimental results

We performed gravity-gradient measurement during two hours integration time. For the measurement, the sign of ΔT was changed after one hour integration time, whereas the direction of the effective wave vector was reversed every measurement cycle. Atomic fringes in configuration ($\pm\Delta T$) are displayed on Fig. 4 when operating the interferometer with total interrogation time $4T = 154.4$ ms. We obtained four spectra in total corresponding to approximately 1800 points per fringe pattern. $\delta\varphi$ is estimated from the fit to the data points for each fringe pattern. The gravity gradient is extracted from the phase offset $\delta\varphi$ considering the four configurations ($\vec{k}_{\text{eff}}$ $\uparrow, \downarrow$, $\pm\Delta T$) leading to four phases ($\delta\varphi_{\uparrow,+}, \delta\varphi_{\uparrow,-}, \delta\varphi_{\downarrow,+}, \delta\varphi_{\downarrow,-}$). Considering the experimental protocol one obtains

$$\Gamma_{zz} = \frac{1}{4}\frac{(\delta\varphi_{\uparrow,+} + \delta\varphi_{\uparrow,-} + \delta\varphi_{\downarrow,+} + \delta\varphi_{\downarrow,-})}{2k_{\text{eff}}v_z T^3 + 4k_{\text{eff}}gT^4} \tag{7}$$

corresponding to an uncorrected gravity gradient of $\Gamma_{zz} =$ 3691 E. The sensitivity of the gradiometer is evaluated from the combined statistical uncertainty from the fitted fringes leading to $\delta\Gamma_{zz} = 2355$ after 2 h integration time. The sensitivity of the measurement using the correlation technique is degraded by a factor of 3 in comparison with the measurement performed in the presence of vibration isolation. First, a decrease by a factor of $\sqrt{2}$ may originate from the use of a fringe scanning (FS) method instead of a more sensitive fringe locking method [43]. Second, degradation of the sensitivity may come from nonperfect correlations due to several factors that we did not have time to investigate, such as misalignment between the classical accelerometer and the AI, unprecise knowledge of the mechanical accelerometer scale factor, uncertainty in the accelerometer transfer function, and bias drift, among others. We estimate the classical accelerometer self-noise to limit our sensitivity at the level of $2\,\text{E}/\sqrt{Hz}$. An improvement of the sensitivity on our measurement is therefore possible. We give in Sec. VII some possible improvements of the method.

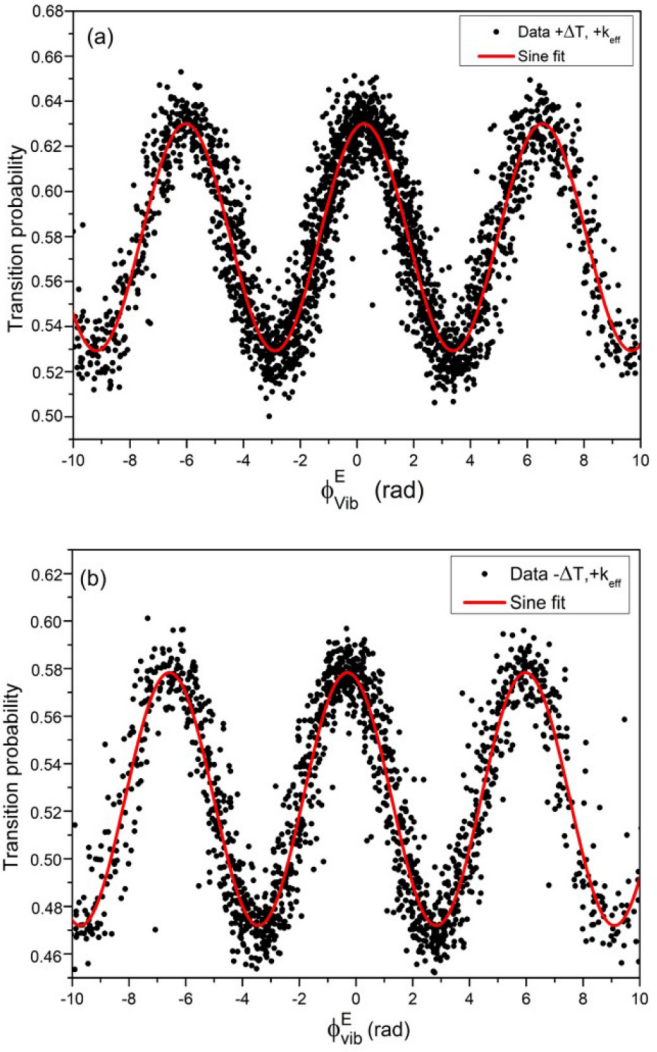

FIG. 4. Measured transition probabilities versus estimated vibration phase calculated from the signal of the classical accelerometer. The atomic gradiometer operates with total interrogation time $4T =$ 154, 4 ms. The solid line is a sinusoidal least-squares fit using Eq. (6). (a) Interference fringes when using $+\Delta T$ timing asymmetry. (b) Interference fringes obtained in the $-\Delta T$ configuration. Two other spectra are obtained reversing the sign of the wave vector.

Systematic effects are studied in the next section.

VI. SYSTEMATIC EFFECTS

In this section we present a study of the main systematics limiting the measurement of the gravity gradient and their related uncertainties.

A. Effect of a slope on fringe offset

In our experiment, we noticed that the fringes obtained by scanning α have a slope on the offset. This slope is due to a change in the resonance condition which appears because of a relatively large fringe spacing ($\propto 1/4T\Delta T$) relative to the fringe envelope ($\propto 1/\tau_{\pi/2}$). The effect can be seen on Fig. 5. This slope is different for each of the four configurations and therefore, when the FLM [17] is used, it is responsible for a

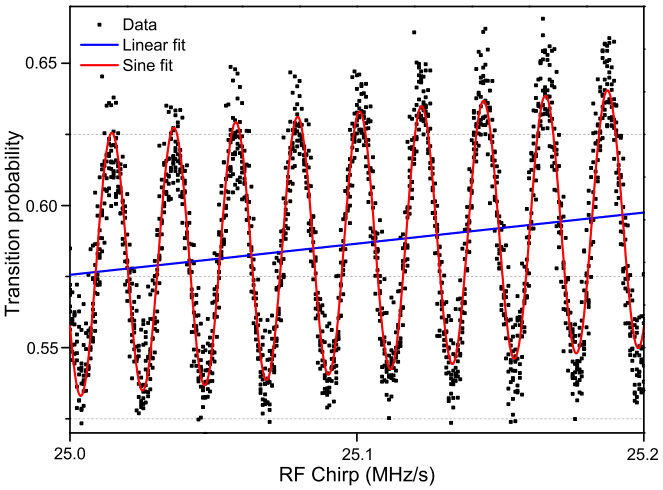

FIG. 5. Effect of slope on fringe offset. The blue line is the estimated fringe offset $P_m = P_{m0} + 2\pi A\alpha$.

bias on the gravity-gradient measurement equal to

$$\Delta\Gamma = \frac{\pi}{24Ck_{\text{eff}}gT^5\Delta T}A, \tag{8}$$

where A is the slope of the fringe offset defined as

$$P_m = P_{m0} + (\alpha - \alpha_0)A. \tag{9}$$

A has been measured for the four configurations of the experiment ($\vec{k}_{\text{eff}}\uparrow,\downarrow,\pm\Delta T$). From these four measurements one can obtain the value of A to estimate the bias:

$$A_{\uparrow,\downarrow,\pm} = \frac{(A_{\uparrow,-} - A_{\downarrow,-}) - (A_{\uparrow,+} - A_{\downarrow,+})}{2}. \tag{10}$$

Using the value of A from Eq. (10), one obtains an estimated bias equal to 4351 E ± 430 E in our configuration.

B. Raman detuning

The nonperfect resonance of the Raman pulses is responsible for a phase shift equal to

$$\begin{aligned}\Delta\Phi_{\text{res}} = \delta\tau &- \text{atan}\left[\frac{\delta+\delta_{LS1}}{\sqrt{\Omega^2+(\delta+\delta_{LS1})^2}}\right.\\ &\left.\times\tan\left(\sqrt{\Omega^2+(\delta+\delta_{LS1})^2}\frac{\tau}{2}\right)\right]\\ &- \text{atan}\left[\frac{\delta+\delta_{LS4}}{\sqrt{\Omega^2+(\delta+\delta_{LS4})^2}}\right.\\ &\left.\times\tan\left(\sqrt{\Omega^2+(\delta+\delta_{LS4})^2}\frac{\tau}{2}\right)\right],\end{aligned} \tag{11}$$

where δ is the two photon Raman detuning in absence of light shift (LS), $\delta_{LS1(4)}$ is the one and two photon light shift at the first (last) pulse, Ω is the effective Rabi pulsation, and τ is the first and last pulse duration. This expression is given for a pulse separation T, $2T$, and T defined between the pulse centers. We notice that this expression is different from a standard MZ AI by the sign between the two atan terms and

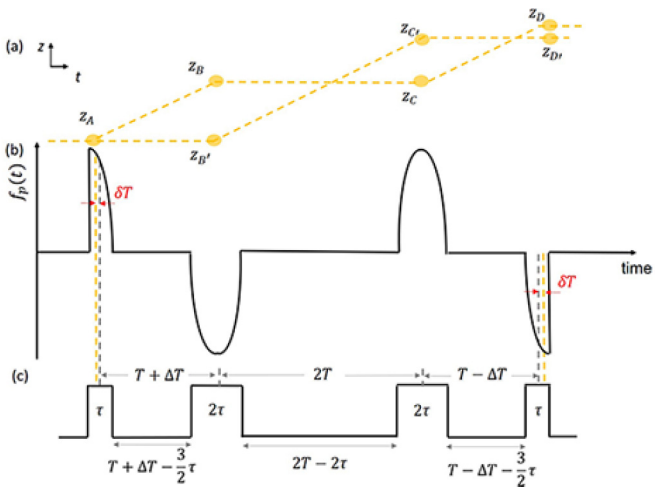

FIG. 6. (a) Space-time diagram of atom classical trajectory for the four pulses AI in absence of gravity. We consider that the path separation occurs at the expected value of the position response during the pulse [$t_{\text{sep}} = \int_0^\tau f_p(t)dt$]. This separation time corresponds to the moment where the laser phase is imprinted on the atom wave function assuming that the laser phase has a linear time dependance during laser pulse. (b) Position response function $f_p(t)$ of the four-pulse AI considering finite Raman pulses [44]. (c) Timing diagram of the four pulse AI defining time with respect to the center of the Raman light pulse.

by the additional terms $\delta\tau$. Thus, contrary to a MZ AI, the effect of Raman detuning does not cancel in a four pulses AI. This effect has thus to be evaluated precisely.

1. *Residual sensitivity to atom velocity*

By assuming $\delta \ll \Omega$, $\pi/2$ pulses ($\Omega\tau = \pi/2$) and neglecting LS, one obtains

$$\Delta\Phi_{\text{res}} = \delta\left(1 - \frac{4}{\pi}\right)\tau. \tag{12}$$

A nonzero detuning and thus a nonresonant atom velocity compared to the Raman transition is responsible for a phase shift. This phase shift can be interpreted as a nonclosed AI (see Fig. 6). To circumvent this effect, one has to add a time shift $\delta T = 1$ μs between the $\pi/2$ pulse and the π pulse.

Thus a time compensation $\delta T = 1$ μs is added to the sequence to compensate for this effect. Nevertheless, experimental defaults such as nonperfect $\frac{\pi}{2}$ pulse or pulse shape asymmetry could affect this timing. We thus measured experimentally the phase shift (see Fig. 7). This was done by varying the time delay at which the radio-frequency chirp α used to compensate the Doppler shift is switched on. One obtains a slope of 3000 E/ms. The uncertainty on the atom velocity is estimated at 1 mm/s leading to an uncertainty on the gravity gradient equal to 300 E.

2. *Light shift*

In our experiment, the one photon light shift is largely canceled by adjusting the intensity ratio between the Raman lasers and using the effective wave-vector reversal protocol. Nevertheless, sensitivity to laser detuning remains through two-photon light shift (TPLS) [45].

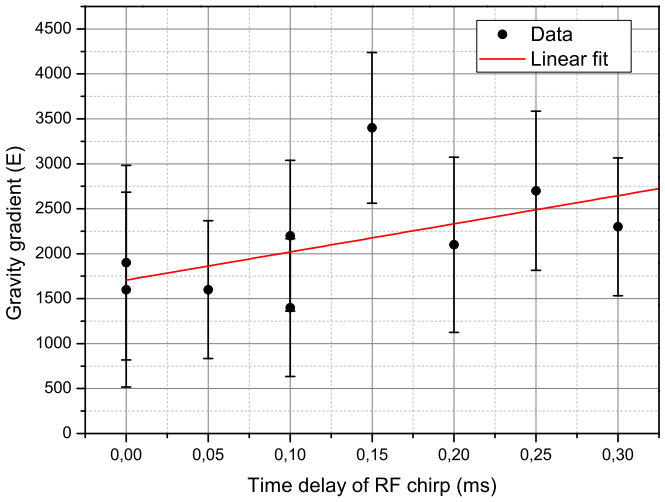

FIG. 7. Gravity-gradient measurement as a function of the time delay to switch on the radio-frequency chirp. The slope given by the linear fit is ≈3000 E/ms.

In our experiment the TPLS is estimated by measuring the gravity gradient as a function of the $\pi/2$ pulse duration keeping effective Rabi frequency constant. For the measurements, the mirror pulses are kept constant to preserve the interferometer's contrast. One can see on Eq. (11) that the phase shift goes to zero when the pulse duration goes to zero regardless the detuning and the effective Rabi frequency. Numerical simulation taking into account the velocity distribution of the atoms shows a linear dependence with the pulse duration with our experimental parameters. Moreover, as the contrast changes with the pulse duration, the measurements are corrected from the slope effect (see Fig. 8). From the linear fit of the measurements we obtained a bias of $\Delta\Gamma = -4351\ \mathrm{E} \pm 2019\ \mathrm{E}$ (uncertainty from the fit).

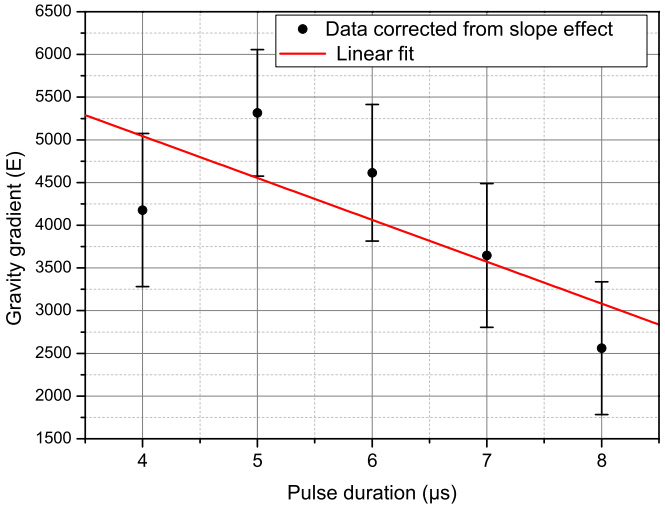

FIG. 8. Variation of the gravity-gradient value due to two-photon light shift (TPLS) versus $\pi/2$-pulse duration keeping Rabi frequency Ω constant. The Raman π pulses are kept constant to preserve the interferometer's contrast. All data points are corrected from the effect of the slope on fringe offset. The slope given by the fit is -490 E/μs.

C. Additional Raman laser lines

Our method of generating the Raman laser by modulation leads to the presence of additional laser lines inducing a supplementary phase shift which, if not corrected, induces an error on the gravity-gradient measurement. We can numerically calculate this supplementary phase shift according to [46] and transposing to the case of a four-pulse AI. In the symmetric configuration of the interferometer ($\Delta T = 0$) it is possible to find an AI configuration where this phase shift is equal to zero. This corresponds to the case where the distance between the position of the atoms at the moment of the four Raman pulses are multiples of the microwave wavelength $\Lambda = c/2\omega_{HFS}$. According to [46] and transposing to the four pulse AI the conditions on interrogation time T and initial velocity of the atoms are given by

$$T = \sqrt{\frac{n\Lambda}{3g}}, \quad v_z = \frac{n'\Lambda - \frac{1}{2}gT^2}{T} \quad \text{with } n, n' \in N. \tag{13}$$

Considering the available free-fall height of 20 cm one finds $n = 2$ and $n' = 1$ leading to $T = 38.6$ ms and initial atomic velocity at first Raman pulse $v_z = gT = 0.38\ \mathrm{ms}^{-1}$. However, timing asymmetry $\Delta T = 300\ \mu$s required one to avoid the presence of extra RB interferometers, changes the atoms position, and prevents one from operating the interferometer in this optimal configuration. We have numerically calculated the error on the gravity gradient for time asymmetry $\Delta T = 300\ \mu$s. This error is a periodic function of the atom-mirror position z_M and is comprised between -300 E and 180 E.

D. Verticality

In our setup, verticality can be ensured with an error of about $\delta\theta = 80\ \mu$rad. As a consequence, supplementary terms in the phase shift arise from the projection of gravity on the horizontal axis which leads to a transverse velocity of the atoms $\delta v = g\delta\theta T$ and a sensitivity to rotation rate with respect to horizontal axis Ω_y. According to [40] this supplementary phase shift is expressed as $\phi = 4k\Omega_y\delta v T^2 = 0.14$ mrad corresponding to an uncertainty of ± 67 E on gravity gradient with Ω_y the Earth rotation rate.

E. Drift of classical accelerometer

The gravity-gradient measurement using the correlation technique is sensitive to errors on the measurement of vibrations such as the bias a_b of the classical accelerometer and its drift $\frac{da_b}{dt}$ during the measurement. We have estimated this drift by measuring the output signal of the accelerometer as a function of time during one day. The bias drift has been estimated from a linear fit to the data to $\frac{da_b}{dt} = -0.47\times10^{-9}$ g/s. From this measurement we have calculated the bias phase induced by the bias drift of our mechanical accelerometer:

$$\varphi_b = 4k_{\mathrm{eff}}\frac{da_b}{dt}T\Delta T T_{\Delta T} + 2k_{\mathrm{eff}}\frac{da_b}{dt}T^3. \tag{14}$$

The first contribution to the bias phase arises from the change in acceleration bias between two measurements performed at ΔT and $-\Delta T$, respectively. In our experimental protocol, the time asymmetry is changed after a time $T_{\Delta T} = 1$ h leading to a bias phase $\simeq 1.26$ mrad corresponding to a bias $\Delta\Gamma = 900$ E.

TABLE II. Correction (Corr.) and uncertainties (u) in Eötvos (E) of the main systematic effects affecting the cold atom gradiometer using two different measurement mehods: (1) vibration isolated; (2) without vibration isolation.

Source	Corr. (1)	u (1)	Corr. (2)	u (2)
Effect of slope	−4351	430		
Two-photon light shift	3920	2019	3920	2019
Sensitivity to initial velocity	0	300	0	300
Additional laser line	0	[−310; 180]	0	[−310; 180]
Verticality	0	67	0	67
Accelerometer drift			−1.5	962
Effect of magnetic field	−100	100	−100	100
Self-attraction effect	−1000	1000	−1000	1000
Statistical u		766		2355
Total	−1531	2459	2818	3428

The second effect arises from the contribution of the drift during the interferometer integration time. This term gives rise to a bias on the gravity-gradient measurement of $\Delta\Gamma = \frac{da_b/dt}{2gT} = 62$ E.

F. Effect of magnetic field

Our interferometer sequence is applied to atoms selected in the $m_F = 0$ state. Nevertheless, a quadratic Zeeman shift and an inhomogeneity in the bias magnetic field applied to the atoms during the interferometer induces an additional phase shift and a bias on the gravity-gradient measurement that can be calculated using [47]. Thanks to our effective wave-vector reversal protocol, this effect is mainly canceled and the associated bias is $\Delta\Gamma = 100\ \text{E} \pm 100\ \text{E}$.

G. Self-attraction effect

Because our experimental setup is not massless, one has to take into account the gravitationnal attraction of the upper part and lower part of the titanium vaccuum chamber on the atomic sensor. The mass difference between the two parts is estimated to $\Delta m = 1.5$ kg. Thus, using a point mass calculation approximation, one can estimate this mass difference to induce an artificial gravity-gradient effect of the form $\Delta\Gamma = \frac{2G\Delta m}{r^3}$, where $G = 6.67\times10^{-11}\,\text{N}\,\text{m}^2\text{kg}^{-2}$ is the gravitational constant and r the distance between the masses. Assuming the distance from the atoms to be between 5 cm and 10 cm the effect is comprised between 1600 E and 200 E, respectively.

H. Conclusion on systematic effects

The results of the main systematics are summarized in Table II. We finally obtained the gravity-gradient values $\Gamma_{zz}^{(1)} = (6069 \pm 2459)$ E and $\Gamma_{zz}^{(2)} = (5173 \pm 3428)$ E, which are statistically in agreement. For both methods the dominant systematic uncertainty comes from TPLS effect. The correlation technique remains limited by statistical uncertainty. Our result is mostly consistent with a measurement performed by a calibrated relative gravimeter (Scintrex CG-3M and CG5) at the location of our experimental setup for different heights, which led to $\Gamma_{zz} = 3180 \pm 30$ E.

TABLE III. Comparison in scale factors $\mathcal{S}$ of Earth-based dual cloud atomic gradiometer with respect to a single-cloud gradiometer. L: apparatus length; g: gravity acceleration; T_{int}: total interrogation time. $T_{\text{int}} = 2T$ $(4T)$ for a Mach-Zehnder type geometry and four-pulse geometry, respectively.

Environment	Mach Zehnder $\mathcal{S}_{MZ}$	Four-pulse AI $\mathcal{S}_{4P}$	Scale factor ratio $\mathcal{S}_{MZ}/\mathcal{S}_{4P}$
Microgravity	$\frac{1}{4}kLT_{\text{int}}^2$	$\frac{1}{32}kLT_{\text{int}}^2$	8
Earth based	$\frac{1}{8}\frac{kL^2}{g}$	$\frac{1}{16}\frac{kL^2}{g}$	2
Earth based + atom launch	$\frac{1}{4}\frac{kL^2}{g}$	$\frac{27}{256}\frac{kL^2}{g}$	≈2.37

VII. DISCUSSION AND POSSIBLE IMPROVEMENTS

We have compared the scale factor ($\mathcal{S} = \partial\Delta\Phi/\partial\Gamma$) of our four pulse AI with the one of a conventional atomic gradiometer using two pairs of Mach-Zehhnder-like atom accelerometers in differential mode. For this comparison we have addressed both Earth-based and space-based (e.g., microgravity) issues. The calculation assumes a total interrogation time T_{int} and apparatus length L. We have neglected the recoil effect term. The recoil term is responsible for a displacement of the atoms that we have assumed to be small compared to the length of the apparatus for our interrogation time. Nevertheless, this term should be considered for long interaction time where the atom displacement is larger. Results are presented in Table III. From Table III, in a microgravity environment, a dual Mach-Zehnder atom accelerometer geometry has a scale factor eight times larger than the one of a four-pulse AI. However, using a single cloud atomic gradiometer for terrestrial applications could be of interest as the reduction in its scale factor is only a factor of 2. This scale factor reduction has to be put in balance with the ease of implementation of such an experimental setup which only requires (i) one atomic source and (ii) an additional Raman π pulse with respect to a conventional Mach-Zehnder atomic gravimeter. One can calculate the gravity-gradient sensitivity $\delta\Gamma$ that can be obtained using the correlation technique and considering an Earth-based gravity-gradient measurement with an interrogation time $T_{\text{int}} = 4T$ corresponding to a 1 m length apparatus. We have taken the case where the atoms are not launched.

Assuming that the ultimate phase resolution is quantum projection noise limited $\delta(\Delta\Phi) \approx 1/\sqrt{N_{at}}$ the single-shot gradiometer sensitivity is given by

$$\delta\Gamma \approx \frac{2}{6C\sqrt{N_{at}}k_{\text{eff}}gT^4}. \tag{15}$$

Assuming 10^6 detected atoms, a total interrogation time of $4T \simeq 452$ ms, and a contrast of $C = 0.5$ which can be obtained with a thermal atomic sample using the adiabatic passage technique [48], one obtains $\delta\Gamma \approx 13\ \text{E}/\sqrt{\text{Hz}}$. This sensitivity can be obtained at the condition that the correlation technique used to bypass the absence of common-mode vibration noise discussed in [23] is not limited by the mechanical accelerometer's sensitivity. The mechanical accelerometer's self-noise has been estimated to $\approx 1\ \text{E}/\sqrt{\text{Hz}}$, and is therefore

not limiting the sensitivity for a typical laboratory environment.

We can expect an improvement of our atomic gradiometer. When using the correlation technique, an increase in sensitivity could be obtained (i) by changing the sign of the timing assymetry ΔT at the repetition rate of the experiment, hence reducing the effect of the classical accelerometer drift by a factor of 3600, and (ii) replacing the fringe fitting procedure by a more sensitive FLM technique using the signal of the classical accelerometer to compensate in real time the phase shift of the AI as in [39]. When measuring the gravity gradient using the vibration isolation platform, applying a phase step $\delta\varphi$ on the Raman laser phase rather than changing the chirp rate α when performing the FLM technique would allow one to cancel the slope effect as the same slope would appear for each of the four fringe patterns. In the scope of field applications, using a single-cloud double-loop AI geometry allows one to be insensitive to Coriolis force [49], which is responsible for both a bias and mostly a severe loss of contrast when performing the AI on a boat [28] or a plane [27] if no rotation compensation is used such as a tip-tilt mirror [50] or a gyrostabilized platform.

VIII. CONCLUSION

In conclusion, we have demonstrated an experimental proof-of-principle measurement of the vertical gravity gradient using a single proof mass of cold ^{87}Rb atoms and a four-pulse double-loop AI. We performed the measurements first using a vibration isolator and then demonstrating the correlation technique in the presence of vibration noise. The results obtained using both methods are in fair agreement despite a reduced sensitivity in comparison with state-of-the-art atomic gradiometers [23,24,26], due to a rather short interrogation time ($4T = 154.4$ ms) and absence of common-mode rejection in a double-loop AI geometry. Better performances of the four-pulse gradiometer are expected with larger interrogation time. Moreover, efficient atom optics techniques such as adiabatic spin-dependent kicks (SDK) [48] could allow enhancement of the gradiometer'sensitivity without need for a colder atomic sample, thus relaxing the complexity of the setup. However, these adiabatic passage techniques still need to be investigated as they may induce uncontrolled phase shifts and therefore additional biases. Finally, in the context of onboard applications, we demonstrated the possibility, in a strap down configuration, to bypass the absence of vibration noise rejection using a correlation technique in combination with a simple experimental setup (one single proof mass and unique detection) with the possibility to switch easily from a gravimeter to a gradiometer immune to constant rotation rate. Despite a reduced sensitivity compared to state of the art setups [51], investigating further the limits of this technique could be of interest for the realization of instruments dedicated to gravity or gradiometry measurements in noisy environments.

ACKNOWLEDGMENTS

We thank F. Nez, from Laboratoire Kastler Brossel (LKB), for discussions on the project. M.C. acknowledges funding from ONERA through Research Project CHAMO (Centrale Hybride AtoMique de l'Onera).

[1] C. J. Bordé, Phys. Lett. A **140**, 10 (1989).
[2] M. Kasevich and S. Chu, Phys. Rev. Lett. **67**, 181 (1991).
[3] R. H. Parker, C. Yu, W. Zhong, B. Estey, and H. Müller, Science **360**, 191 (2018).
[4] R. Bouchendira, P. Cladé, S. Guellati-Khélifa, F. Nez, and F. Biraben, Phys. Rev. Lett. **106**, 080801 (2011).
[5] J. B. Fixler, G. T. Foster, J. M. McGuirk, and M. A. Kasevich, Science **315**, 74 (2007).
[6] G. Rosi, F. Sorrentino, L. Cacciapuoti, M. Prevedelli, and G. M. Tino, Nature (London) **510**, 518 (2014).
[7] S. Fray, C. A. Diez, T. W. Hänsch, and M. Weitz, Phys. Rev. Lett. **93**, 240404 (2004).
[8] A. Bonnin, N. Zahzam, Y. Bidel, and A. Bresson, Phys. Rev. A **88**, 043615 (2013).
[9] D. Schlippert, J. Hartwig, H. Albers, L. L. Richardson, C. Schubert, A. Roura, W. P. Schleich, W. Ertmer, and E. M. Rasel, Phys. Rev. Lett. **112**, 203002 (2014).
[10] M. G. Tarallo, T. Mazzoni, N. Poli, D. V. Sutyrin, X. Zhang, and G. M. Tino, Phys. Rev. Lett. **113**, 023005 (2014).
[11] L. Zhou, S. Long, B. Tang, X. Chen, F. Gao, W. Peng, W. Duan, J. Zhong, Z. Xiong, J. Wang, Y. Zhang, and M. Zhan, Phys. Rev. Lett. **115**, 013004 (2015).
[12] P. Hamilton, M. Jaffe, P. Haslinger, Q. Simmons, H. Müller, and J. Khoury, Science **349**, 849 (2015).
[13] T. Kovachy, P. Asenbaum, C. Overstreet, C. Donnelly, S. M. Dickerson, A. Sugarbaker, J. M. Hogan, and M. A. Kasevich, Nature (London) **528**, 530 (2015).
[14] A. Peters, K. Y. Chung, and S. Chu, Metrologia **38**, 25 (2001).
[15] P. Gillot, O. Francis, A. Landragin, F. Pereira Dos Santos, and S. Merlet, Metrologia **51**, L15 (2014).
[16] Z. K. Hu, B. L. Sun, X. C. Duan, M. K. Zhou, L. L. Chen, S. Zhan, Q. Z. Zhang, and J. Luo, Phys. Rev. A **88**, 043610 (2013).
[17] Y. Bidel, O. Carraz, R. Charrière, M. Cadoret, N. Zahzam, and A. Bresson, Appl. Phys. Lett. **102**, 144107 (2013).
[18] M. Hauth, C. Freier, V. Schkolnik, A. Senger, M. Schmidt, and A. Peters, Appl. Phys. B **113**, 49 (2013).
[19] T. L. Gustavson, P. Bouyer, and M. A. Kasevich, Phys. Rev. Lett. **78**, 2046 (1997).
[20] A. Gauguet, B. Canuel, T. Lévèque, W. Chaibi, and A. Landragin, Phys. Rev. A **80**, 063604 (2009).
[21] G. Tackmann, P. Berg, C. Schubert, S. Abend, M. Gilowski, W. Ertmer, and E. M. Rasel, New J. Phys. **14**, 015002 (2012).
[22] I. Dutta, D. Savoie, B. Fang, B. Venon, C. L. G. Alzar, R. Geiger, and A. Landragin, Phys. Rev. Lett. **116**, 183003 (2016).
[23] J. M. McGuirk, G. T. Foster, J. B. Fixler, M. J. Snadden, and M. A. Kasevich, Phys. Rev. A **65**, 033608 (2002).

[24] F. Sorrentino, Q. Bodart, L. Cacciapuoti, Y.-H. Lien, M. Prevedelli, G. Rosi, L. Salvi, and G. M. Tino, Phys. Rev. A **89**, 023607 (2014).
[25] X.-C. Duan, M.-K. Zhou, D.-K. Mao, H.-B. Yao, X.-B. Deng, J. Luo, and Z.-K. Hu, Phys. Rev. A **90**, 023617 (2014).
[26] P. Asenbaum, C. Overstreet, T. Kovachy, D. D. Brown, J. M. Hogan, and M. A. Kasevich, Phys. Rev. Lett. **118**, 183602 (2017).
[27] R. Geiger, V. Ménoret, G. Stern, N. Zahzam, P. Cheinet, B. Battelier, A. Villing, F. Moron, M. Lours, Y. Bidel, A. Bresson, A. Landragin, and P. Bouyer, Nat. Commun. **2**, 474 (2011).
[28] Y. Bidel, N. Zahzam, C. Blanchard, A. Bonnin, M. Cadoret, A. Bresson, D. Rouxel, and M.-F. Lequentrec-Lalancette, Nat. Commun. **9**, 627 (2018).
[29] O. Carraz, C. Siemes, L. Massotti, R. Haagmans, and P. Silvestrin, Micrograv. Sci. Technol. **26**, 139 (2014).
[30] M. N. Nabighian, M. E. Ander, V. J. S. Grauch, R. O. Hansen, T. R. Lafehr, Y. Li, W. C. Pearson, J. W. Peirce, J. D. Phillips, and M. E. Ruder, Geophysics **70**, 63ND (2005).
[31] C. Jekeli, Navigation **52**, 1 (2005).
[32] M. Langlois, R. Caldani, A. Trimeche, S. Merlet, and F. Pereira dos Santos, Phys. Rev. A **96**, 053624 (2017).
[33] M. Cadoret, E. de Mirandes, P. Cladé, S. Guellati-Khélifa, C. Schwob, F. Nez, L. Julien, and F. Biraben, Phys. Rev. Lett. **101**, 230801 (2008).
[34] B. Estey, Ph.D. thesis, University of California, Berkeley, 2016, Chap. 5.
[35] J. F. Clauser, Physica B **151**, 262 (1988).
[36] K. Chung, Ph.D. thesis, Stanford University, 2001, Chap. 5.
[37] J. K. Stockton, K. Takase, and M. A. Kasevich, Phys. Rev. Lett. **107**, 133001 (2011).
[38] S. Merlet, J. L. Gouët, Q. Bodart, A. Clairon, A. Landragin, F. Pereira Dos Santos, and P. Rouchon, Metrologia **46**, 87 (2009).
[39] J. Lautier, L. Volodimer, T. Hardin, S. Merlet, M. Lours, F. Pereira Dos Santos, and A. Landragin, Appl. Phys. Lett. **105**, 144102 (2014).
[40] M. Cadoret, N. Zahzam, Y. Bidel, C. Diboune, A. Bonnin, F. Théron, and A. Bresson, J. Opt. Soc. Am. B **33**, 1777 (2016).
[41] F. Théron, O. Carraz, G. Renon, N. Zahzam, Y. Bidel, M. Cadoret, and A. Bresson, Appl. Phys. B **118**, 1 (2015).
[42] B. Barrett, L. Antoni-Micollier, L. Chichet, B. Battelier, P.-A. Gominet, A. Bertoldi, P. Bouyer, and A. Landragin, New J. Phys. **17**, 085010 (2015).
[43] X.-C. Duan, D.-K. Mao, X.-B. Deng, M.-K. Zhou, C.-G. Shao, Z. Zhu, and Z.-K. Hu, Chin. Phys. B **27**, 013701 (2018).
[44] A. Bonnin, Ph.D. thesis, University of Paris-Saclay, 2015, Chap. 1.
[45] P. Cladé, E. de Mirandes, M. Cadoret, S. Guellati-Khélifa, C. Schwob, F. Nez, L. Julien, and F. Biraben, Phys. Rev. A **74**, 052109 (2006).
[46] O. Carraz, R. Charrière, M. Cadoret, N. Zahzam, Y. Bidel, and A. Bresson, Phys. Rev. A **86**, 033605 (2012).
[47] P. Storey and C. Cohen-Tannoudji, J. Phys. II (France) **4**, 1999 (1994).
[48] M. Jaffe, V. Xu, P. Haslinger, H. Müller, and P. Hamilton, Phys. Rev. Lett. **121**, 040402 (2018).
[49] K. P. Marzlin and J. Audretsch, Phys. Rev. A **53**, 312 (1996).
[50] S.-Y. Lan, P.-C. Kuan, B. Estey, P. Haslinger, and H. Müller, Phys. Rev. Lett. **108**, 090402 (2012).
[51] D. DiFrancesco, A. Grierson, D. Kaputa, and T. Meyer, Geophys. Prospect. **57**, 615 (2009).